Combustion and Flame 159 (2012) 2474–2479

Contents lists available at SciVerse ScienceDirect

Combustion and Flame

journal homepage: www.elsevier.com/locate/combustflame

Thermite powder ignition by localized microwaves

Yehuda Meir, Eli Jerby *

Faculty of Engineering, Tel Aviv University, Ramat Aviv 69978, Israel

ARTICLE INFO

Article history:
Received 3 October 2011
Received in revised form 10 January 2012
Accepted 12 February 2012
Available online 10 March 2012

Keywords:
Thermite
Microwave heating
Hotspots
Thermal runaway
Ignition

ABSTRACT

This paper presents a new method to ignite pure thermite powder by low-power microwaves (~100 W). In this method, the microwave energy is supplied locally to the powder. It creates a confined hotspot, and initiates a self-propagating combustion in the entire powder volume. The coupled thermal–electromagnetic interaction evolved within the powder prior to its ignition is simulated theoretically, taking into account the powder's temperature-dependent parameters. The simulation results show a thermal-runaway instability and localized heating within a confined hotspot, induced mostly by the microwave's electric-field component. The experimental setup employs accordingly an open-end applicator implemented by a miniature solid-state microwave-drill device inserted into the thermite powder as a local igniter. The experimental results show ignition within ~3 s at 2.1-GHz, 100-W microwave injection, in agreement with the theoretical model. The dependence of the minimal microwave power on the exposure time required to reach combustion is identified. Practical aspects and potential applications of this mechanism, such as rust conversion, energy production, and propulsion are indicated.

1. Introduction

Exothermic thermite reactions occur between metal-oxides and metals in powder mixtures. For example, the reaction between magnetite and aluminum [1],

$$3Fe_3O_4 + 8Al \rightarrow 9Fe + 4Al_2O_3 + 3.67\ \text{kJ/g}, \tag{1}$$

produces iron and alumina, and releases energy comparable to TNT explosion. Thermite reactions are of interest for a variety of applications, such as explosives (e.g. for automotive air-bag safety systems), cutting and welding of metals, and processing of ceramics and composite materials [2–4]. The thermite reaction is an environmental-friendly energy source [5], and it can be utilized as a fuel in oxygen-free environments such as underwater due to the inherent zero oxygen balance of the thermite reaction (1).

The thermite's flame temperature (4057 K theoretically in ideal adiabatic conditions [6]) is significantly higher than that of hydrocarbon fuels. However, it is much harder to ignite thermite than common explosives [7]. This difficulty is alleviated in practice by additives (e.g. calcium peroxide) [8] which reduce the ignition temperature of the thermite, but also deteriorate its quality. Hence, there is a considerable motivation to develop practical means to ignite pure thermites.

Laser beams were found effective for ignition of thermite powders [9]. Pre-heating of thermites also improves their combustion speeds [10]. Electrostatic discharges were studied as a means to ignite aluminum powders [11]. Thermite ignition by high-power microwaves was reported using a 75-GHz, 50 kW gyrotron pulse [12]. In more general, microwaves were found effective for flame enhancement and stabilization [13]. A volumetric ignition of Fe_3O_4–Al thermite by a magnetic (H-field) coupling in a 2-kW microwave cavity was investigated as a means to initiate self-propagating high-temperature synthesis (SHS) for sintering of ceramic composites [14]. The magnetic (H-field) coupling of microwaves to powders made of non-magnetic metals was discovered as an effective heating mechanism [15]. This permeability-like effect in the macroscopic level is attributed to the eddy currents induced in the metallic particles [16].

The intentional concentration of microwave energy into a small hotspot (much smaller than the microwave's wavelength) within the heated object was studied in the context of the microwave-drill invention [17]. The microwave's self-focusing mechanism involves a thermal-runaway instability in which the dissipated energy is confined within the hotspot, hence the localized heating accelerates its temperature rise [18] and leads inevitably to the hotspot's phase transition (e.g. melting, evaporation, or breakdown [19]). This localized microwave-heating mechanism is studied experimentally and theoretically in the next sections as a means to ignite pure thermite powders.

2. Conceptual scheme

A simplified scheme of the localized microwave applicator employed for the thermite ignition in this study is illustrated in

---

* Corresponding author.
E-mail address: jerby@eng.tau.ac.il (E. Jerby).

0010-2180/$ - see front matter © 2012 The Combustion Institute. Published by Elsevier Inc. All rights reserved.
doi:10.1016/j.combustflame.2012.02.015

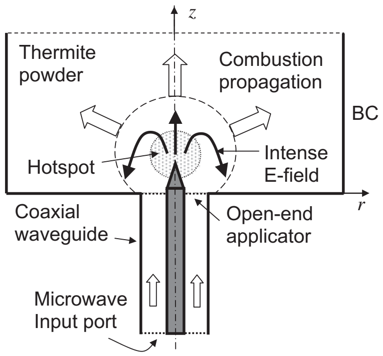

Fig. 1. A conceptual illustration of the thermite powder ignition by localized microwaves radiated by an open-end applicator. The tip inserted into the powder concentrates the electric-field lines intensely, and creates a hotspot by a thermal-runaway instability. The thermite is heated locally up to its ignition temperature. Once ignited, the self-sustained combustion propagates in the entire powder volume (BC denotes boundary conditions presented in Section 3).

Fig. 1. The microwave energy is delivered by a coaxial waveguide to an open-end applicator with a center electrode slightly inserted into the thermite powder. As in the microwave-drill interaction [17], the self-focused microwave energy is absorbed mostly near the center-electrode tip hence the electric field is most intense there (this localization effect is not significantly affected by the powder's further boundary conditions). Consequently, a thermal-runaway process is evolved and a hotspot is formed there within the thermite mixture. The thermally unstable hotspot evolved is heated up to the thermite's ignition temperature, thus initiating a self-propagating combustion process within the entire volume of the thermite powder.

3. Localized microwave-heating simulation

The pre-combustion heating phase of the thermite ignition is modeled here by the coupled thermal–electromagnetic equations [18]. The simulation model imported from Ref. [18] is extended here to include the magnetic heating effect (neglected in Ref. [18]) in addition to the electric-field heating. The model is applied here to the thermite powder in the 2-D circularly-symmetrical geometry illustrated in Fig. 1. The processed material is situated in an open metallic box, represented by boundary conditions (BC) of a perfect electric conductor (PEC) for the electromagnetic (EM) wave. The EM wave is irradiated locally via the coaxial applicator. The thermal BC is presented by a thin metal wall surrounded by air hence it is almost isolated due to the relatively small heat convection through it.

The coupled EM-wave and heat equations are presented in a two-time-scale approach in the form

$$\nabla \times [(\mu_r' - j\mu_r'')^{-1}\nabla \times \tilde{\mathbf{E}}] - [\varepsilon_r' - j(\varepsilon_r'' + \sigma/\omega\varepsilon_0)]k_0^2\tilde{\mathbf{E}} = 0, \tag{2}$$

$$\rho C_p \partial T/\partial t - \nabla \cdot (k_{th}\nabla T) = Q, \tag{3}$$

where the dependent variables are $\tilde{\mathbf{E}}$, the electric-field vector component of the EM wave, and T, the temperature, both in r–z coordinates. The electric field is presented in the frequency domain, where ω and k_0 are its angular frequency and free-space wave-number, respectively. The thermite powder is represented by its temperature-dependent parameters, μ_r, ε_r, σ, ρ, C_p, and k_{th}, where $\mu_r = \mu_r' - j\mu_r''$ and $\varepsilon_r = \varepsilon_r' - j\varepsilon_r''$ are its complex relative magnetic permeability and dielectric permittivity, respectively, and σ is its electric conductivity. In the heat equation (3), ρ, C_p and k_{th} are the density, the heat capacity, and the thermal conductivity, respectively, of the relevant material at each point (the analysis takes into account the actual parameters of the thermite powder, the tungsten electrode, and the surrounding air).

The temperature T is varying slowly with respect to the EM wave. The distinction between the typical time scales of the EM wave propagation (~1 ns) and the slower thermal evolution (>1 ms) allows the *two-time scale* approximation. Its validity is verified by the heuristic condition $\rho C_p d_{hs}^2/k_{th} \gg \tau$, where d_{hs} is the hotspot width and $\tau = 2\pi/\omega$ is the wave period. The EM bandwidth is sufficiently narrow to neglect any parametric variation with frequency hence the wave equation (2) is solved in the frequency domain while the heat equation (3) is computed in the slowly-varying time domain. Eqs. (2) and (3) are coupled together by the local EM heat dissipation,

$$Q = \frac{1}{2}\left[(\sigma + \omega\varepsilon_0\varepsilon_r'')|\tilde{\mathbf{E}}|^2 + \omega\mu_0\mu_r''|\tilde{\mathbf{H}}|^2\right], \tag{4}$$

and by the consequent variations in the material's parameters due to the temperature rise. The second term in the right-hand side of Eq. (4) represents the magnetic heating, where $\tilde{\mathbf{H}} = j(\omega\mu_0\mu_r)^{-1}\nabla \times \tilde{\mathbf{E}}$ is the magnetic vector components of the EM field. As the temperature rises, the spatial variations in ε_r, μ_r and σ modify the microwave radiation pattern hence enabling the self-focusing effect. The temperature evolution is initiated at room temperature uniformly in the entire region. Since the simulation does not include phase changes, it is halted at the melting temperature of the aluminum component of the mixture (933 K).

The temperature-dependent parameters of the mixed powder (namely its thermal conductivity, heat capacity, density, permittivity, and permeability) are estimated by the parameters of its raw ingredients, taking into account the particle sizes and mixing ratio. The powder simulation employs the Heat-Transfer and Radio-Frequency (RF) modules of the COMSOL Multiphysics® software package. The temperature-dependent parameters of the aluminum powder component ε_{r1}, μ_{r1} are derived from [20] for mono-sized 37 μm diameter spheres in a body centered cubic (BCC) structure, in the relevant temperature range. Its thermal conductivity is derived by simulating the temperature gradient generated by a steady-state heating of a thin layer of aluminum powder, with boundary conditions of a constant temperature on one surface and a constant heat flux on the other one. Its heat capacity is simulated by a uniform heating source within isolating boundary conditions.

The temperature-dependent permittivity and permeability of the magnetite powder, ε_{r2}, μ_{r2}, are imported from the literature for <75 μm [21] and 38–62 μm [22] particle-size powders at high density. Their thermal-conductivity and heat-capacity parameters are taken from [23] and [24], respectively. The dielectric loss-tangent of the magnetite varies from 0.07 at room temperature to 1.0 at 900 K. The aluminum powder exhibits a smaller absorption in magnetic coupling, and its dielectric coupling is negligible here. The thermite mixture is simulated as a homogeneous powder of spherical aluminum and magnetite particles uniformly distributed in a 1:1 volumetric fraction ratio. The contact resistance between the powder's particles [25] is assumed to be negligibly large (simulated as small air gaps between particles). The weighted complex permittivity and permeability of the thermite mixture are derived by Lichtenecker logarithmic mixture rule [26], as

$$\varepsilon_r = \sqrt{\varepsilon_{r1}\varepsilon_{r2}}, \quad \mu_r = \sqrt{\mu_{r1}\mu_{r2}}. \tag{5a, b}$$

Figure 2 shows the resulted dielectric and thermal parameters of the thermite powder in the range from room temperature up to the aluminum melting point (933 K). The results show that the dielectric loss increases and the thermal conductivity decreases with the temperature rise, hence enabling the thermal-runaway instability induced by the electric field component. The effect of the different particle sizes presented in Fig. 2a for two size

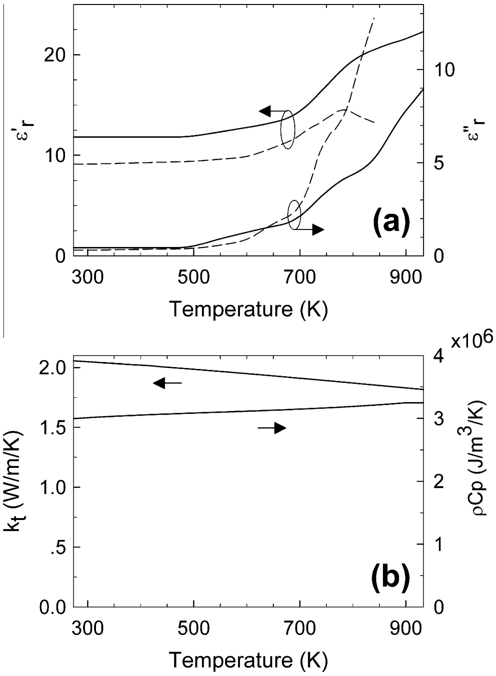

Fig. 2. Estimated temperature-dependent properties of a thermite powder composed of an aluminum–magnetite mixture: (a) the complex dielectric permittivity, and (b) the thermal conductivity and volumetric heat capacity. The solid and dashed curves in (a) refer to mixtures consisting of <75 μm [21] and 38–62 μm [22] magnetite size distributions, respectively.

distributions in the micron range is relatively small, and both are sufficiently susceptible for microwave ignition. The effects of the particle size and shape, and of the powder density, on the microwave properties of magnetite were explored recently [27]. The particle size has a much more significant effect on the thermite combustion rate, in the self-propagating phase evolved after the microwave ignition phase. The self-burning rate then is faster for smaller particle sizes, as shown in Ref. [28]. The contact resistance is also more significant for smaller particles [25] hence increasing the heating rate in finer powders due to the larger dissipated power. The contact resistivity is affected also by deformation and necking effects, as in metallic powder sintering by DC heating [29].

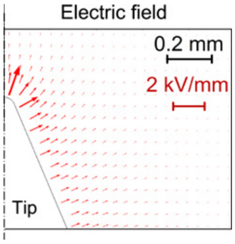

Fig. 3. A simulation result of the initial vectorial electric-field distribution within the thermite powder in a 100-W microwave input power. (For interpretation to colours in this figure, the reader is referred to the web version of this paper.)

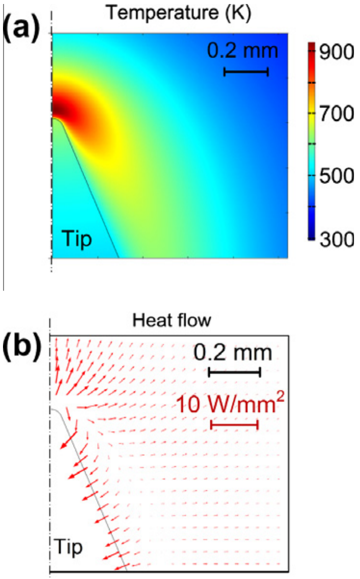

Fig. 4. Simulation results of the microwave heating at 100-W input power, reaching the aluminum melting temperature (933 K) near the tip after 3 s. (a) The temperature distribution. (b) The heat flow originated from the hotspot. (For interpretation to colours in this figure, the reader is referred to the web version of this paper.)

The temperature profile evolution during the thermite microwave heating is simulated accordingly using COMSOL Multiphysics® for a mixture made of <75 μm magnetite and 37 μm aluminum powders. Figure 3 shows the vectorial distribution of the initial electric field for a 100-W, 2.45-GHz microwave input power at room temperature. The electric field exceeds 2×10^6 V/m locally in front of the electrode tip. The EM wave is attenuated in the lossy medium, but it does not propagate further also because of the decoupled polarization and the cutoff condition in this case. The cylindrical-cup diameter $D = 0.02$ m is sufficiently narrow with respect to the EM-wave wavelength, $\lambda_{Th} = 0.05$ m in the thermite, to satisfy the cutoff condition for a circular waveguide [30] given by

$$D < \frac{p'_{11}}{\pi} \lambda_{Th}, \tag{6}$$

where $p'_{11} = 1.84$ is the first zero of the first-order Bessel function derivative, $J'_1(p'_{11}) = 0$. Hence the wave becomes evanescent and it decays a few millimeters away from the tip.

Simulation results of the localized heating effect induced within the thermite powder in a thermal-runaway process are presented in Fig. 4a and b. The simulated temperature distribution after 3 s is shown in Fig. 4a. The localized hotspot confinement is clearly seen in front of the electrode tip. The heat flow from the ~0.1-mm hotspot towards the powder bulk, and the ridge shape due to the electrode cooling effect, are clearly seen in the vectorial heat-flux plot in Fig. 4b.

The temperature rise shown in Fig. 5 exhibits the thermal-runaway instability in the thermite powder E-field heating, in accord with its dielectric-loss increase and thermal conductivity decrease with temperature (Fig. 2). Consequently, after 3 s the heating rate exceeds 1000 K/s and the thermite reaches the melting temperature of its aluminum component (933 K). For the sake of comparison between electric and magnetic heating, the open-end applicator is replaced by a short-end coaxial structure with a magnetic half-loop coupler inserted into the powder. The simulation result presented in Fig. 5 (dashed curve) for the H-field heating shows an initial magnetic heating rate of 800 K/s, faster than the initial E-field heating. However, the magnetic heating slows down above 800 K to a rate of 100 K/s, attributed to the magnetite's Curie temperature at 858 K [21]. The magnetic heating does not exhibit thermal-runaway instability like the electric heating, which accelerates much faster at high temperatures. The electric heating is found to be more effective above the magnetite's Curie temperature for the further heating required to reach the thermite's ignition temperature (>1773 K). Hence, the electric-coupling is considered as a preferable mechanism in this case for thermite ignition (note a similar conclusion for a pure magnetite heating in Ref. [22]).

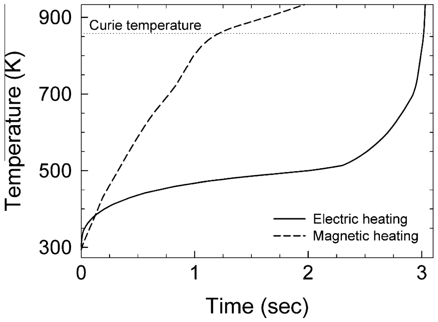

Fig. 5. The peak temperature evolution vs. time in electrically-induced localized heating (solid curve) leading to the results shown in Fig. 4a and b. The thermal-runaway instability is evident by the accelerated temperature increase and by the hotspot confinement in front of the electrode tip (shown in Fig. 4a). For the sake of comparison, the dashed curve shows the magnetic-coupling heating at the same input power. The initial rate of the magnetic heating is higher but it slows down significantly above the Curie point of the magnetite.

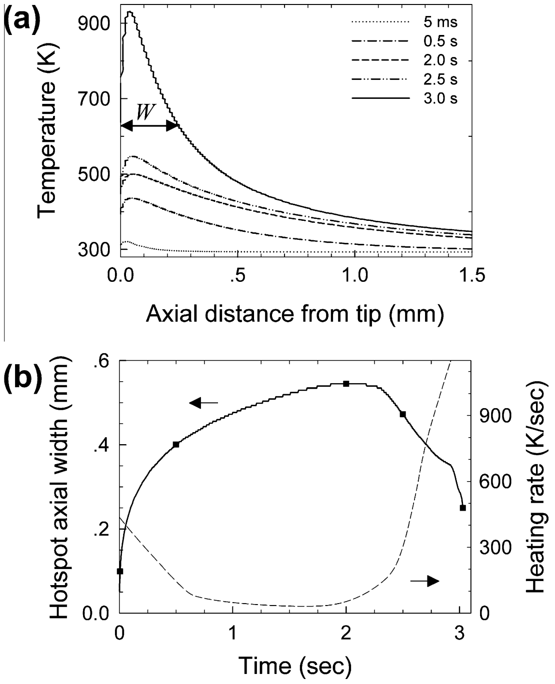

Fig. 6. The spatial and temporal hotspot evolution. (a) The temperature profile evolution in time. (b) The hotspot's axial width evolution with respect to the heating rate (the dots indicate the times presented in Fig. 6a). The hotspot relative shrinkage is associated with the heating rate increase.

Figure 6a shows the temperature profile of the hotspot along the z axis in front of the tip, as evolved in successive times in E-field heating (associated with Fig. 5 solid curve). The hotspot's axial width is defined here by the axial distance from the tip in which the temperature attains one half of its peak temperature, as denoted by W in the upper curve in Fig. 6a. The temporal evolution of the axial width W is presented in Fig. 6b with the heating rate (the time derivative of the temperature curve in Fig. 5). The inverse relation between the two is clearly seen. At the initial heating, the hot region tends to expand and the heating rate decreases in time, but once the thermal-runaway instability emerges (after ~2 s) these tendencies are exchanged. The hotspot starts to shrink relatively while the heating rate is accelerating simultaneously towards ignition.

In summary, the main assumptions made in this model are the following:

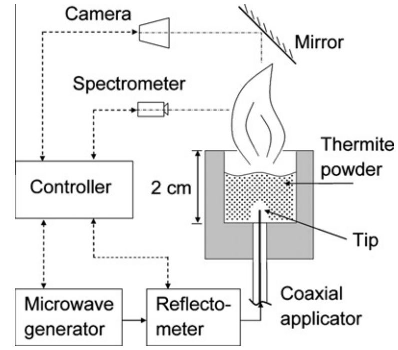

Fig. 7. The experimental setup of the microwave thermite igniter, including a power-controlled 140-W solid-state microwave-generator, a reflectometer, and a coaxial applicator. The diagnostics is provided by a video camera and by an optical spectrometer. The dashed arrows indicate the signal lines connected to a PC LabVIEW controller.

a. The thermite is composed of a magnetite powder as in Ref. [21] mixed with mono-sized 37 μm aluminum spherical particles (as in Ref. [20]) in an equal volumetric ratio.
b. The contact resistance between particles is assumed to be negligibly large.
c. The particle sizes of both ingredients are assumed to be in the order of 10–100 μm according to the relevant parameters available in the literature [21,22].
d. The Lichtenecker's logarithmic mixture rule (Eqs. (5a, b)) is applicable.
e. The rapid temperature increase continues above the aluminum melting point up to the thermite ignition by the thermal-runaway instability hence the ignition time can be extrapolated accordingly (e.g. in Fig. 5).

4. Experimental setup and results

The experimental setup depicted in Fig. 7 employs a solid-state microwave oscillator at 2.1 GHz, and an open-end coaxial applicator (a miniature microwave-drill device [31,32]) inserted into the powder as a local low-power igniter. The miniature 140-W oscillator consists of an LDMOS transistor circuit (Freescale MRF 6S21140 evaluation board) with a power control. The 2-cm diameter of the inner ignition chamber is filled with a 2-g batch of thermite powder. The cutoff condition (6) is satisfied thus the microwave initiates the ignition but the wave becomes evanescent away from the tip, and it does not affect the self-propagating volumetric combustion (note also that the energy released by the thermite combustion is much larger than the microwave energy spent to ignite it, hence the latter is negligible after ignition). The microwave cutoff allows us also to open the outer chamber upside with no microwave leakage, thus the reaction can be viewed directly, photographed, and detected by an optical spectrometer. The microwave-generator's controls, as well as the incident and reflected microwave signals, are monitored and sampled by a LabVIEW interface for further analyzes.

The thermite powder employed in this study is made of a mixture of Aluminum-400 powder (~37 μm particle size) and Black-318 (<45 μm particle size) iron-oxide Fe_3O_4 powder (>93% purity) in a stoichiometric ratio of 1:3.2 by weight, respectively. A typical flame of the magnetite–aluminum thermite ignited in this setup is shown in Fig. 8a and b, in side and top-view images, respectively. The iron and alumina product of this combustion is shown in Fig. 8c.

The experimental results of 26 runs accumulated in Fig. 9 display the incident microwave power and the corresponding

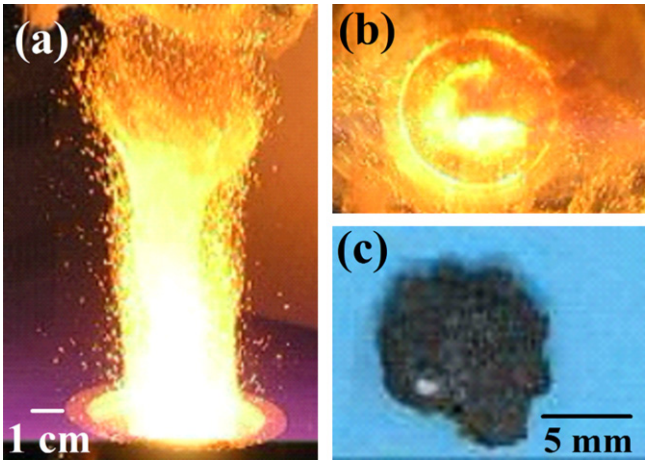

Fig. 8. A typical flame of Fe_3O_4–Al thermite ignited by localized microwaves in the setup depicted in Fig. 7. The optical images show the side (a) and top-view (b) of the flame, and its alumina and iron product (c). (For interpretation to colours in this figure, the reader is referred to the web version of this paper.)

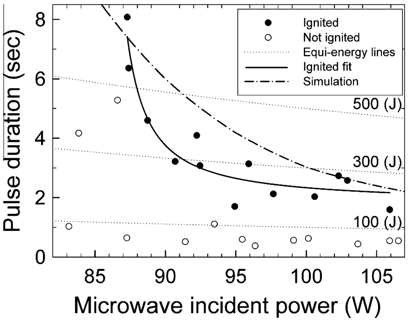

Fig. 9. Time-to-ignite measurements of Fe_3O_4–Al thermite powder by varying the pulse duration with respect to the microwave incident power. The experimental curve fit (using the function $y = a\exp[b/(x + c)]$) is compared to the theoretical curve resulted from the numerical simulation, and to equi-energy contours.

exposure-time duration required to reach combustion in this setup. The comparison presented with the theoretical simulation results assumes that the ignition occurs in a relatively short time after reaching the steep thermal-runaway instability in the simulation (e.g. at 3.03 s in Fig. 5). The microwave reflection measurements in these experiments indicate that the net effective power absorbed by the powder is ~0.5 of the incident power. The successful results of complete thermite burning are fitted by the solid line, which represents the lower bound of the incident microwave power required for the thermite ignition in this setup. The hyperbolic dotted curves mark equi-energy pulses of constant microwave power and exposure time products. These show the advantage of the relatively high-power (>100 W) short pulses (<3 s) which require less energy per pulse (<300 J) to ignite the thermite powder. The non-ignited cases are shown as well in order to verify this lower bound. The thermite mixture failed to ignite also with unmatched sizes of aluminum and magnetite. For example, running the experiment with smaller aluminum particles of 18 μm (instead of 37 μm) with the same magnetite (>75 μm as before), the microwave heating causes local burning of the powder as before, but it does not evolve to self-propagating combustion (hence the different conditions for the two distinct phases, of (a) the microwave localized heating, and (b) the self-propagating combustion [28]).

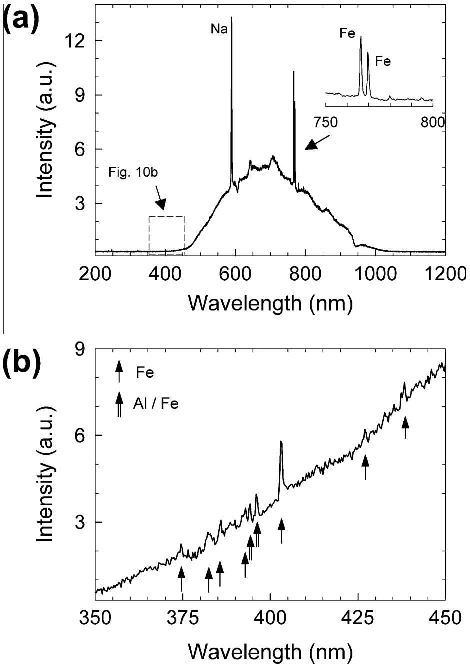

Fig. 10. The optical spectrum of the thermite combustion ignited by localized microwaves. (a) Using an iris to reduce intensity, the two dominant lines of iron are revealed at 766 and 770 nm. (b) Removing the iris, additional lines of iron are revealed in the unsaturated 350–450 nm region. The lines at 394 and 396 nm can be attributed also to aluminum in the given 0.3-nm spectral resolution.

Optical spectroscopy measurement enables to identify the iron generated in the ejected thermite flame [33]. Figure 10 presents the optical spectrum detected during the thermite combustion by an Avantes AvaSpec-3648 spectrometer (14 Hz sampling rate, 0.3 nm resolution). An iris is installed in front of the spectrometer in order to suppress the intense blackbody radiation emitted by the thermite combustion, and to avoid saturation in the main spectral range. The two dominant lines of iron are observed at 766 nm and 770 nm. Removing the iris enables to focus on the lower intensity (unsaturated) region of the spectrum in the range 350–450 nm, revealing a multiple line of iron at 403 nm. Other two lines, at 394 nm and 396 nm, can be attributed to aluminum or to iron within the 0.3 nm resolution ambiguity. Additional weaker lines of iron seem to emerge from the background at 375 nm, 382 nm, 386 nm, 393 nm, 427 nm, and 438 nm. Hence, the spectral measurement supports the experimental validation of the thermite reaction.

The energy released by the 2-g batch of thermite in these experiments may exceed 7 kJ theoretically, which is >20 times larger than the microwave energy spent to ignite it. This ignition efficiency can be improved further by incorporating an adaptive impedance-matching mechanism in the setup. Microwave excited plasma as in Ref. [34] may also accelerate the ignition process. The thermite combustion can be made more efficient also by using smaller particle size powders, in the nanometer scale, in order to enlarge the reactant surface area between the particles, and to improve their mass transport diffusion which is crucial for the diffusion-limited thermite combustion [28,35]. The stoichiometric ratio is found to be a significant parameter for the combustion speed in thermite, as in Ref. [36].

5. Conclusions

The theory and experiments presented in this paper introduce the ignition effect of pure thermite powder of micron-size particles with no additives by a relatively low microwave power (<100 W) in an effectively unbounded space. These results provide a basis for a practical method to ignite pure thermite powders for applications in various scales (from a ~1-g batch and larger).

Depending on the coupling by an open or short-end applicator, the microwave absorption by the thermite is attributed either to the electric or to the magnetic field component, respectively. As seen in Fig. 5, the magnetic heating can be more effective in the lower temperature range, below the Curie point, whereas the dielectric heating elevates more rapidly above the thermal-runaway turning point (at ~700 K) up to the thermite's ignition temperature (>1773 K) [37]. Hence, in order to expedite the ignition, one may conceive a sequential combination of the magnetic and electric heating in a two-stage applicator. In this arrangement, the magnetic pre-heating will be applied first by a magnetically-coupled applicator, which will become electrically-coupled by varying its geometry in order to enable the further heating more rapidly. This sequential mechanism can be implemented by a fusible short-end loop, or by a movable electrode. This approach may shorten the ignition process significantly.

The thermite ignition method presented here is studied further also for applications of melting, cutting, and welding of various metals, for localized direct conversion of rusty surfaces to iron (note that the thermite reaction of rust and aluminum produces iron and alumina similarly to (1)), and as a fuel in oxygen-free environments. A comprehensive model shall include the contact resistance and necking effects between the powder particles (e.g. as in Refs. [38,39]). These further studies will be presented in future publications. The low-power microwave ignition technique presented above enables solid-state embodiments of various thermite igniters in compact, low-cost, silent, automatic and portable devices. The various versatile implementations of this concept may open new possibilities for the practical applications mentioned above and for material processing, explosive charge detonation, coating, sintering and various SHS processes, as well as combustion and propulsion applications.

Acknowledgment

This research is supported by the Israel Science Foundation under Grant No. 1639/11.

References

[1] L. Durães, J. Campos, A. Portugal, Prop. Explos. Pyrotech. 31 (2006) 42–49.
[2] B. Ho, S. Chang-qing, Key Eng. Mater. 419–420 (2010) 393–396.
[3] Q.S. Meng, S.P. Chen, J.F. Zhao, H. Zhang, H.X. Zhang, Z.A. Munir, Mater. Sci. Eng. A 456 (2007) 332–336.
[4] L.L. Wang, Z.A. Munir, Y.M. Maximov, J. Mater. Sci. 28 (1993) 3693–3708.
[5] G. Cao, R. Orrù, Chem. Eng. J. 87 (2002) 239–249.
[6] S.H. Fischer, M.C. Grubelich, in: Proc. 24th Int'l Pyrotechnics Seminar, Monterey, CA, 1998.
[7] K.C. Patil, S.T. Aruna, S. Ekambaram, Curr. Opin. Solid State Mater. Sci. 2 (1997) 158–165.
[8] V. Kobyakov, L. Mashkinov, M. Sichinava, High Temp. 47 (2009) 119–122.
[9] M.L. Mileham, M.P. Kramer, A.E. Stiegman, J. Phys. Chem. C 111 (2007) 16883–16888.
[10] B. Dikici, M.L. Pantoya, V. Levitas, Combust. Flame 157 (2010) 1581–1585.
[11] E. Beloni, E.L. Dreizin, Combust. Flame 157 (2010) 1346–1355.
[12] G.M. Batanov, N.K. Bereghetskaya, V.A. Kopiev, I.A. Kossyi, A.N. Magunov, V.A. Shcherbakov, N.V. Sachkova, Dokl. Phys. 51 (2006) 180–185.
[13] E.S. Stockman, S.H. Zaidi, R.B. Miles, C.D. Carter, M.D. Ryan, Combust. Flame 156 (2009) 1453–1461.
[14] C.C. Lee, N. Yoshikawa, S. Taniguchi, J. Mater. Sci. 46 (2011) 7004–7011.
[15] J. Cheng, R. Roy, D. Agrawal, J. Mater. Sci. Lett. 20 (2001) 1561–1563.
[16] M. Ignatenko, M. Tanaka, M. Sato, Jpn. J. Appl. Phys. 48 (2009) 067001-1–067001-6.
[17] E. Jerby, V. Dikhtyar, O. Aktushev, U. Grosglick, Science 298 (2002) 587–589.
[18] E. Jerby, O. Aktushev, V. Dikhtyar, J. Appl. Phys. 97 (2005) 034909-1–034909-7.
[19] V. Dikhtyar, E. Jerby, Phys. Rev. Lett. 96 (2006) 045002-1–045002-4.
[20] T. Galek, K. Porath, E. Burkel, U. van Rienen, Model. Simul. Mater. Sci. Eng. 18 (2010) 025015-1–025015-13.
[21] Z. Peng, J.Y. Hwang, J. Mouris, R. Hutcheon, X. Huang, ISIJ Int. 50 (2010) 1590–1596.
[22] M. Hotta, M. Hayashi, K. Nagata, ISIJ Int. 51 (2011) 491–497.
[23] J. Mølgaard, W.W. Smeltzer, J. Appl. Phys. 42 (1971) 3644–3647.
[24] J.P. Coughlin, E.G. King, K.R. Bonnickson, J. Am. Chem. Soc. 73 (1951) 3891–3893.
[25] G.R. Ruschau, S. Yoshikawa, R.E. Newnham, J. Appl. Phys. 72 (1992) 953–959.
[26] R. Simpkin, IEEE Trans. Microw. Theory Tech. 58 (2010) 545–550.
[27] M. Hotta, M. Hayashi, A. Nishikata, K. Nagata, ISIJ Int. 49 (2009) 1443–1448.
[28] J.J. Granier, M.L. Pantoya, Combust. Theory Model. 8 (2004) 555–565.
[29] J.R. Groza, A. Zavaliangos, Mater. Sci. Eng. A 287 (2000) 171–177.
[30] R.E. Collin, Foundation for Microwave Engineering, third ed., McGraw Hill, 2001.
[31] Y. Meir, A. Salzberg, E. Jerby, Hotspot induced by low-power microwave drill – transistor-based localized heaters and their new applications, in: Proc. Ampere 13th Int'l Conf., September 5–8, 2011, Toulouse, France, pp. 201–204.
[32] Y. Meir, E. Jerby, Proc. COMCAS-IEEE Int'l Conf., November 7–9, 2011, Tel Aviv, Israel, pp. 1–4.
[33] Y. Meir, E. Jerby, Microw. Opt. Technol. Lett. 53 (2011) 2281–2283.
[34] E. Jerby, A. Golts, Y. Shamir, S. Wonde, J.B.A. Mitchell, J.L. LeGarrec, T. Narayanan, M. Sztucki, D. Ashkenazi, Z. Barkay, Appl. Phys. Lett. 95 (2009) 191501-1–191501-3.
[35] J.L. Cheng, H.H. Hng, H.Y. Ng, P.C. Soon, Y.W. Lee, J. Phys. Chem. Solids 71 (2010) 90–94.
[36] K.B. Plantier, M.L. Pantoya, A.E. Gash, Combust. Flame 140 (2005) 299–309.
[37] M. Stir, K. Ishizaki, S. Vaucher, R. Nicula, J. Appl. Phys. 105 (2009) 124901-1–124901-4.
[38] A.V. Gusarov, E.P. Kovalev, Phys. Rev. B 80 (2009) 024202-1–024202-15.
[39] E. Beloni, P.R. Santhanam, E.L. Dreizin, J. Electrostat. 70 (2012) 157–165.